



Stemflow dissolved organic matter in mixed temperate forests: temporal and interspecific variation of optical indices and development of a stemflow-specific PARAFAC model

Robyn C. O'Halloran · Jennifer J. Guerard ·
Delphis F. Levia

Received: 15 November 2023 / Accepted: 13 June 2024 / Published online: 21 June 2024
© The Author(s) 2024

Abstract Stemflow is a conduit for the transport of canopy-derived dissolved organic matter (DOM) to the forest floor. This study examined the character of stemflow DOM for four tree species over four phenophases (leafless, emergence, leafed, and senescence for deciduous species and leafed-winter, emergence, leafed- spring/summer, and senescence for coniferous species) occurring in temperate forests; namely, *Betula lenta* L. (sweet birch), *Fagus grandifolia* Ehrh. (American beech), *Liriodendron tulipifera* L. (yellow poplar), and *Pinus rigida* Mill. (pitch pine). American beech exhibited the lowest average specific UV

absorbance at 254 nm ($SUVA_{254}$) values, while yellow poplar displayed the highest values. $SUVA_{254}$ values were largest in senescence and smallest in emergence. The spectral slope ratio was lower for pitch pine than the deciduous tree species. Humification index (HIX) values decreased across all species during the emergence phenophase. The developed and validated stemflow-specific four-component parallel factor analysis (PARAFAC) model demonstrated the combined influence of interspecific and temporal fluctuations on the composition of humic and protein-like substances within stemflow. By separating and examining stemflow DOM independent of throughfall, our study provides fresh insights into the spatiotemporal dynamics of stemflow inputs to near-trunk soils that may inform hot spots and hot moments theories.

Responsible Editor: Jacques C. Finlay

Supplementary Information The online version contains supplementary material available at <https://doi.org/10.1007/s10533-024-01158-8>.

R. C. O'Halloran · D. F. Levia (✉)
Department of Civil & Environmental Engineering,
University of Delaware, Newark, DE, USA
e-mail: dlevia@udel.edu

J. J. Guerard
Department of Chemistry, United States Naval Academy,
Annapolis, MD, USA

D. F. Levia
Department of Geography & Spatial Sciences, University
of Delaware, Newark, DE, USA

D. F. Levia
Department of Plant & Soil Sciences, University
of Delaware, Newark, DE, USA

Keywords Dissolved organic matter · Stemflow · Carbon cycling · Fluorescence spectroscopy · Phenophase

Introduction

Throughfall and stemflow are important pathways for the transfer of water, solutes, and particulates to the forest floor (Parker 1983; Levia et al. 2011, 2023; Levia and Germer 2015; Siegert et al. 2017; Chen et al. 2019; Cayuela et al. 2019). Similar to throughfall (McDowell et al. 2020), stemflow mediates the

transfer of dissolved organic matter (DOM) from tree canopies to the forest floor, helping to shape biogeochemical cycling in wooded ecosystems (e.g., Levia et al. 2012; Ryan et al. 2022). Due to the high aqueous solubility and mobility of DOM, it is leached and transported from the foliage, bark, and twigs via throughfall and stemflow, thereby enriching the surrounding ecosystem (Van Stan et al. 2017; McDowell et al. 2020). As a spatially localized input (e.g., Carlyle-Moses et al. 2018; Llorens et al. 2022), stemflow can impact soil moisture levels, groundwater recharge, as well as the composition and functioning of the soil microbial community (Levia and Germer 2015).

Characterization of absorbance spectral indices have been reported for throughfall and stemflow of a variety of deciduous and coniferous species, including *Acer saccharum* Marsh. (sugar maple), *Betula alleghaniensis* Britt. (yellow birch), *Fagus grandifolia* Ehrh. (American beech), *Liriodendron tulipifera* L. (yellow poplar), *Juniperus virginiana* L. (eastern red cedar), *Picea abies* L. (Norway spruce), and *Pinus sylvestris* L. (Scots pine) (Inamdar et al. 2012; Levia et al. 2012; Cooper et al. 2016; Stubbins et al. 2017; Van Stan et al. 2017; Thieme et al. 2019; Wagner et al. 2019; Ryan et al. 2022). These studies reported throughfall and stemflow specific UV absorbance at 254 nm ($SUVA_{254}$) values within the range of 1.6 to 6.2 L mg-C⁻¹ m⁻¹, demonstrating that the distribution between aliphatic vs. aromatic compounds vary among tree species. However, few studies (Levia et al. 2012; Ryan et al. 2022) have reported absorbance ratios at 250:365 nm ($E_2:E_3$), spectral slope, or spectral slope ratio (S_R) values for throughfall and stemflow, finding that these characterizations may be associated with soluble lignin degradation byproducts and humic acid isolates in stemflow. Such data are valuable because stemflow plays an important role in shaping the dynamics of the soil carbon cycle and groundwater recharge (Levia and Germer 2015). Variations in these metrics among tree species, especially within individual storms, could exert notable impacts on the temporal dimension of biogeochemical reactivity in near-trunk soils (Levia et al. 2012).

Some studies have reported fluorescence characterization using parallel factor analysis (PARAFAC) modeling of both stemflow and throughfall samples, finding that throughfall and stemflow DOM consists of humic-like, fulvic-like and protein-like

components (Cooper et al. 2016; Van Stan et al. 2017; Thieme et al. 2019; Ryan et al. 2022). The distribution of the components differ between the tree species examined, emphasizing the impact of species-specific processes. For sugar maple, yellow birch, and Bahamas pine, Cooper et al. (2016) and Ryan et al. (2022) found the fluorescence index (FI) and biological index (BIX) were consistent with terrestrial, aromatic, tree-derived sources.

A few studies have analyzed the temporal variation of stemflow DOM absorbance (Levia et al. 2012; Van Stan et al. 2017; Ryan et al. 2022). These studies examined differences in stemflow DOM within individual rainfall events (Levia et al. 2012), among rainfall events (e.g., Van Stan et al. 2017), between leafed and leafless states (Levia et al. 2012), from mature green to senescence to leafless states (Ryan et al. 2022), and with or without epiphyte coverage (Van Stan et al. 2017). Ryan et al. (2022) determined that climatic and seasonal effects impacted the character of the DOM components as a function of the leafed and senescence seasons. However, the relationship between DOM composition and these processes is not fully understood, especially stemflow DOM quality with respect to phenophase and carbon cycling in forest ecosystems.

The objective of this study is to quantify the absorbance and fluorescence signatures of stemflow DOM for four major tree species throughout different phenophases (i.e., leafless, emergence, leafed, and senescence for deciduous species and leafed-winter, emergence, leafed- spring/summer, and senescence for coniferous species) of a temperate eastern forest of the United States. Our emphasis on stemflow is partly motivated by its localized nature to forest soils (e.g., Levia and Germer 2015; Michalzik et al. 2016; Llorens et al. 2022) which can engender the creation of hot spots in the proximal area of tree trunks. For instance, the median DOC flux-based stemflow enrichment ratio (expressed per unit trunk basal area) for yellow birch was 72 as compared to 6 for the throughfall flux-based enrichment ratio, illustrating the potential for stemflow to influence forest soils (Ryan et al. 2022). To the authors' knowledge, this is the first study to characterize the optical spectroscopy of stemflow DOM in relation to four different phenophases, developing a *solely* stemflow-based PARAFAC model. Analyzing stemflow DOM independently from throughfall promotes a deeper interpretation of

its chemical composition, which may improve understanding surrounding the creation of localized hot spots and hot moments in near-trunk soils.

Materials and methods

Study area

This study was conducted within the Fair Hill Natural Resources Management Area in Cecil County, Maryland, USA (39° 42' N, 75° 50' W). Situated in the Chesapeake Bay watershed, the site has an average elevation of 70 m above sea level (Siegert et al. 2016). The region experiences a continental climate characterized by hot and humid summers, as well as mild to cool winters, featuring well-defined seasons. Annual mean high and low air temperatures are 19.1 °C and 7.2 °C, respectively, with an average annual precipitation of 1193 mm for the period from 1991 to 2020 (U.S. Climate Normals 2023). The summer months (July through September) typically constitute the driest period, while spring (April through June) emerges as the wettest season (Siegert et al. 2016). The geological substrate of the study area is the metamorphic Mt. Cuba Wissahickon Formation, predominantly comprised of pelitic gneiss and schist, with minor occurrences of pegmatite and amphibolite. Soil classification places it within the Glenelg series, characterized by its deep, well-drained nature and moderate topography. The valley soils are Oxyaquic Dystrudepts, occasionally experiencing seasonal water saturation, while the shallower hillside soils may be characterized as loamy, mixed, mesic Lithic Dystrudepts. Geologically, the site falls within the Piedmont geologic regime of the Mid-Atlantic region (Inmadar et al. 2012).

Vegetation primarily consists of a deciduous forest, complemented by a small *Pinus rigida* Mill. (pitch pine) community. Notable tree species include *Liriodendron tulipifera* L. (yellow poplar), *Fagus grandifolia* Ehrh. (American beech), and *Betula lenta* L. (sweet birch). Canopy trees in the study area exhibit a mean tree height of 27.8 m, a stand density of 225 trees ha⁻¹, a stand basal area of 36.8 m² ha⁻¹, and an average diameter at breast height (dbh) of 40.8 cm (Levia et al. 2010). To account for the full diameter range of each tree species at the study site, care was taken to collect stemflow from trees of all diameters

over the course of study. The dbh range of trees sampled for each species is as follows: American beech 14.2 to 65.3 cm, sweet birch 14.3 to 49.0 cm, yellow poplar 17.9 to 79.0 cm, and pitch pine from 27.7 to 46.6 cm. It is important to note that the bark morphology differs among the four test species. Whereas mature yellow poplar and pitch pine are rough-barked species with furrows and ridges in the bark, American beech is a smooth-barked species without furrowed bark. The bark of sweet birch consists of a platy structure that has smoother surfaces with some fissures between plates. Its bark roughness increases with tree size as the smoother bark of smaller trees becomes more platy and more fissures develop between the platy structures.

Field instrumentation and sample collection

Stemflow collars, crafted from plastic tubing, were affixed to each tree, with the tubing length customized based on tree circumference (measured from dbh). The tubing was halved lengthwise and sealed to the tree using silicone sealant to ensure a watertight connection. The remaining uncut tubing was linked to a 121 L high-density polyethylene container. New polyethylene plastic bags were put in the stemflow collection bins just prior to each sampled rain event. Stemflow was collected over a 14-month period. Stemflow was collected in clean 1 L amber jars that were rinsed with stemflow water specific to each tree before sample collection. These samples were filtered on the same day to prevent degradation and stored at 4 °C for subsequent analysis. To confirm that polyethylene bags did not impact carbon analyses, we introduced 18 MΩ ultrapure water (Milli-Q, Millipore, Burlington MA, USA) into the bags, subjected them to agitation, allowed them to stand for 24 h, filtered them, and conducted carbon concentration analysis. The results revealed no significant changes.

Dissolved organic carbon (DOC)

Following determination of electrical conductivity and pH (WTW ProfiLine pH/Cond 3320 Multiparameter Meter), samples were vacuum-filtered through a 0.7 μm, 47 mm glass fiber filter (Whatman GF/F 1825-047) (Shigihara et al. 2008). Filtered samples were analyzed for non-purgeable organic carbon (NPOC), akin to dissolved organic carbon (DOC),

using a Shimadzu TOC-LCSH/CSN (Shimadzu, Kyoto, Japan) with the 680 °C combustion catalytic oxidation method and quantified against a 100 mg L⁻¹ standard prepared from a 1000 µg mL⁻¹ total organic carbon standard solution (Thermo Scientific, Specpure®), with auto-dilutions ranging from 2 to 100 mg L⁻¹. Stemflow DOC concentrations were analyzed over a 14-month period.

Stemflow optical properties

Optical properties of stemflow were measured for samples collected over a 14-month period. Filtered DOC samples were diluted with 18 MΩ ultrapure water (Milli-Q, Millipore, Burlington MA, USA) to 10 mg-C L⁻¹ to ensure the absorbance was less than 1.0 to prevent inner filter light screening effects (IFE) (Kalbitz et al. 2000). The ultraviolet (UV)-visible absorbance spectrum (Fig. S1) was analyzed every 1 nm from 200 to 800 nm on an Agilent Cary 60 UV-Vis Spectrophotometer (Agilent Technologies,

Inc., Santa Clara, California) with a 1-cm quartz cuvette. Specific ultraviolet absorbance (SUVA₂₅₄), spectral slope ratio (S_R), and E₂:E₃ were determined using the equations in Table 1.

Stemflow DOM fluorescence was measured on a Horiba Scientific Aqualog (Horiba Instruments, Edison, NJ, USA) with a 1-cm quartz cuvette of filtered samples diluted to an absorbance less than 1. Excitation-emission matrices (EEMs) were scanned using excitation from 200 to 600 nm, every 3 nm and emission from 200 to 600 nm every 4 px (2.33 nm) (Fig. S2). EEMs were blank subtracted using 18 MΩ ultrapure water, and prior to export corrected for IFE in the Aqualog software v. 4.0. FI, humification index (HIX), BIX, and freshness index (β:α) were determined using the equations in Table 1.

Statistical analysis

Parallel factor analysis (PARAFAC) was employed to model EEM spectra to resolve the fluorescent

Table 1 Absorbance and fluorescence characterization and description of variables adapted from Inamdar et al (2012) and Hansen et al. (2016)

| | Equation | Description | Source |
|--------------------------------|--|---|--|
| Absorbance | | | |
| SUVA ₂₅₄ | $\frac{abs_{254}}{[DOC]/100}$ | abs ₂₅₄ = absorbance at 254nm [DOC] = concentration of DOC of the sample (mg-C/L) 1/100 = pathlength in m | Weishaar et al. (2003) |
| S _R | $\log\left(\frac{S_{275-295}}{S_{350-400}}\right)$ | S ₂₇₅₋₂₉₅ /S ₃₅₀₋₄₀₀ = slope of the absorbance between wavelength 275 nm to 295 nm and 350 nm to 400 nm, respectively | Helms et al. (2008) |
| E ₂ :E ₃ | $\frac{abs_{250}}{abs_{365}}$ | abs ₂₅₀ = absorbance at 250nm abs ₃₆₅ = absorbance at 365nm | Peuravuori and Pihlaja (1997) |
| Fluorescence | | | |
| FI | $\frac{I_{370,470}}{I_{370,520}}$ | I _{370,470} /I _{370,520} = Intensity at 370 nm excitation and 470 nm or 520 nm emission, respectively | McKnight et al. (2001); Cory et al. (2010) |
| HIX | $\frac{\sum I_{254,435-480}}{\sum I_{254,300-345} + \sum I_{254,435-480}}$ | $\sum I_{254,435-480} / \sum I_{254,300-345}$ = The summation of intensities at excitation 254 nm from 435 to 480 nm and 300 nm to 345 nm emission, respectively | Ohno (2002) |
| BIX | $\frac{I_{310,380}}{I_{310,430}}$ | I _{310,380} /I _{310,430} = Intensity at 310 nm excitation and 380 nm or 430 nm emission, respectively | Huguet et al. (2009) |
| β:α | $\frac{I_{310,280}}{MAX(I_{310,280}, I_{310,346})}$ | I _{310,280} = Intensity at 310 nm excitation and 280 nm emission MAX(I _{310,280} , I _{310,346}) = Maximum intensity at 310 nm excitation and between 280 and 246 nm emission | Parlanti et al. (2000); Wilson and Xenopoulos (2009) |

components in stemflow DOM using the StaRdom package (Pucher et al. 2019) in R v. 4.2.2. Raman and Rayleigh scattering were removed as well as excitation wavelengths below 250 nm and emission wavelengths above 580 nm to minimize noise outside the spectral range of interest. A total of 153 EEMs from sampled stemflow DOM were normalized to their maximum fluorescence intensity to prevent high correlation from low fluorescence signals. A 4-component model (Fig. S3) converged explaining 99.3% of fluorescent data and was validated by both split-half analysis (Fig. S4) with Tucker's congruence coefficient > 0.99 for all samples and also by random initialization, to ensure results are global rather than local minima (Stedmon and Bro 2008).

General descriptive statistics, including maxima, minima, average, median, and standard deviation, were calculated for stemflow DOC concentrations as well as optical properties ($SUVA_{254}$, S_R , $E_2:E_3$, FI, HIX, BIX, $\beta:\alpha$, %C1, %C2, %C3, and %C4). Significant (p -value < 0.05) differences between the species were determined for DOC concentrations and optical properties using the Kruskal–Wallis one way ANOVA with ranks due to a non-normal distribution of the stemflow data. When the Kruskal–Wallis test determined a significant finding among the four tree species, the post hoc Dunn's test for multiple pairwise comparison with the Bonferroni adjustment,

was employed to identify statistically significant differences between specific tree species. The analysis sequence also was performed for phenophase comparisons within the dataset. Statistical analyses were conducted in SigmaPlot v. 15.0.

Results

Dissolved organic carbon

DOC was analyzed with respect to both species and phenophase (Fig. 1). Each species' lowest average DOC concentrations occurred during emergence. Yellow poplar and sweet birch both displayed the highest average DOC concentration during the leafed phenophase (Fig. 1; Table S1). For American beech, senescence had the highest DOC concentration ($19.05 \text{ mg L}^{-1} \pm 11.34$). Pitch pine showed a marked difference only between emergence and the other three phenophases, with emergence being roughly half that of the other phenophases (Fig. 1; Table S1).

Optical properties: absorbance

Absorbance characteristics across species and phenophase showed distinctive patterns for each spectral index (Tables 2 and 3). American beech exhibited the

Fig. 1 Average DOC concentration for each tree species (American beech, sweet birch, yellow poplar, and pitch pine) and grouped by phenophase (leafless/leafed—winter, emergence, leafed/leafed—spring/summer, senescence), with error bars displaying 95% confidence intervals

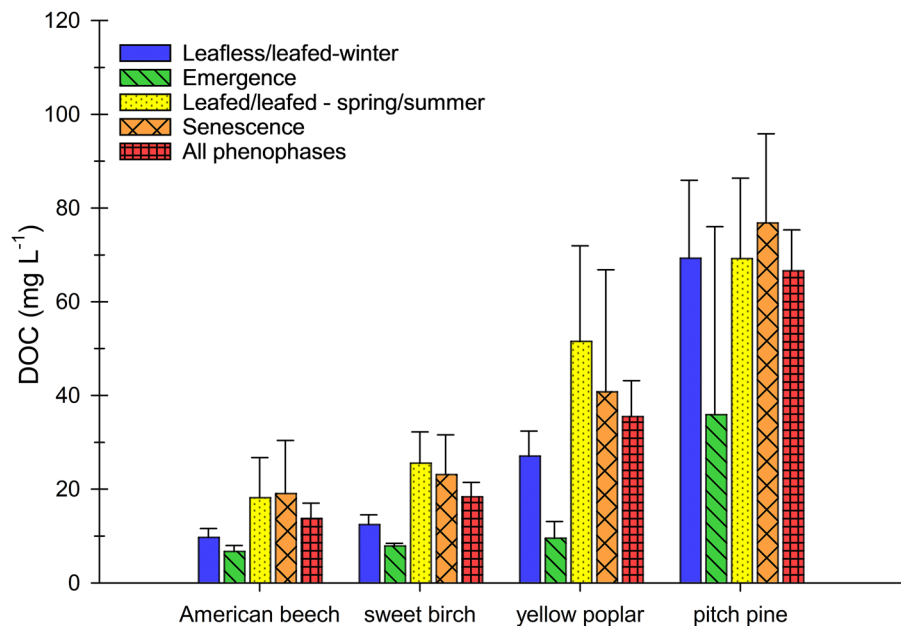


Table 2 Average tree species-specific absorbance and fluorescence characterization with 95% confidence intervals, all phenophases combined

| | American beech ($n=41$) | Sweet birch ($n=39$) | Yellow poplar ($n=37$) | Pitch pine ($n=36$) |
|--|------------------------------|------------------------|--------------------------|-----------------------|
| SUVA ₂₅₄ (L mg C ⁻¹ m ⁻¹) | 2.55 ± 0.42 | 2.66 ± 0.36 | 4.15 ± 0.60 | 3.91 ± 0.44 |
| E ₂ :E ₃ | 4.51 ± 0.11 | 4.80 ± 0.22 | 5.59 ± 0.18 | 4.79 ± 0.13 |
| S _R | 1.17 ± 0.02 | 1.17 ± 0.03 | 1.28 ± 0.02 | 1.02 ± 0.02 |
| FI | 1.51 ± 0.02 | 1.44 ± 0.02 | 1.38 ± 0.01 | 1.31 ± 0.02 |
| HIX | 0.71 ± 0.06 | 0.73 ± 0.06 | 0.75 ± 0.06 | 0.69 ± 0.06 |
| β:α | 0.50 ± 0.02 | 0.45 ± 0.01 | 0.52 ± 0.01 | 0.43 ± 0.02 |
| BIX | 0.52 ± 0.04 | 0.49 ± 0.05 | 0.52 ± 0.01 | 0.43 ± 0.01 |

Table 3 Average phenophase-specific absorbance and fluorescent characterization with 95% confidence intervals, all tree species combined

| | Leafless / leafed -winter ($n=69$) | Emergence ($n=12$) | Leafed / Leafed— spring/summer ($n=54$) | Senescence ($n=18$) |
|--|---|----------------------|---|-----------------------|
| SUVA ₂₅₄ (L mg C ⁻¹ m ⁻¹) | 3.01 ± 0.36 | 2.31 ± 0.61 | 3.43 ± 0.47 | 4.50 ± 0.33 |
| E ₂ :E ₃ | 5.07 ± 0.17 | 4.79 ± 0.21 | 4.83 ± 0.17 | 4.74 ± 0.21 |
| S _R | 1.18 ± 0.03 | 1.13 ± 0.05 | 1.15 ± 0.03 | 1.14 ± 0.05 |
| FI | 1.38 ± 0.02 | 1.42 ± 0.03 | 1.44 ± 0.03 | 1.44 ± 0.04 |
| HIX | 0.73 ± 0.05 | 0.45 ± 0.17 | 0.76 ± 0.05 | 0.76 ± 0.04 |
| β:α | 0.44 ± 0.01 | 0.53 ± 0.06 | 0.51 ± 0.01 | 0.48 ± 0.02 |
| BIX | 0.45 ± 0.01 | 0.53 ± 0.06 | 0.55 ± 0.04 | 0.48 ± 0.03 |

lowest mean SUVA₂₅₄ values (2.55 L mg C⁻¹ m⁻¹), while yellow poplar displayed the highest values (Table 2). SUVA₂₅₄ values indicate two distinct groups among tree species (p -value ≤ 0.0001 , Dunn's test), with American beech and sweet birch having mean SUVA₂₅₄ values < 3 and pitch pine and yellow poplar with SUVA₂₅₄ values > 3.9 . Phenophases exhibited substantial variation, with the highest mean SUVA₂₅₄ values observed during senescence (4.50 L mg C⁻¹ m⁻¹) and the lowest during emergence (2.31 L mg C⁻¹ m⁻¹) (Table 3). There was minimal variance ($\sigma^2=0.006$) observed between the leafed/leafed-spring/summer and leafless/leafed-winter conditions.

Yellow poplar exhibited the highest E₂:E₃ value, whereas American beech displayed the lowest with statistically significant distinctions observed across species (p -value < 0.0001 , Dunn's test) with the one exception of pitch pine and sweet birch (p -value = 0.661, Dunn's test) (Table 2). The leafless/leafed-winter phenophase had the highest E₂:E₃ value

at 5.07, a notable deviation from the other phenophases (ranging from 4.74 to 4.83) (Table 3).

S_R exhibits a differing pattern in comparison to E₂:E₃ and SUVA₂₅₄ across various species, with groupings related to tree-classification (deciduous vs. coniferous) (Table 2). Notably, the conifer pitch pine, which had one of the higher SUVA₂₅₄ values along with yellow poplar, did *not* have a higher S_R, unlike yellow poplar (average S_R for pitch pine is 1.02, compared to 1.17, 1.17, and 1.28; p -value pitch pine vs yellow poplar/American beech/sweet birch < 0.0001 , Dunn's test, p -value yellow poplar/American beech/sweet birch range 0.112 to 0.293, Dunn's test) (Table 2).

Optical properties: interspecific and phenophase comparisons among indices

EEMs of the four tree-species (Fig. S1) revealed significant interspecific differences in FI values (p -value < 0.0001 , one-way ANOVA) (Table 2).

American beech exhibited the highest mean FI at 1.51, while pitch pine displayed the lowest at 1.31, consistent with the DOM deriving primarily from trees. Among the deciduous species, BIX values did not significantly differ (p -value = 0.2950, one-way ANOVA) and maintained an approximate mean value of ~0.50 (Table 2). Conversely, pitch pine BIX was significantly lower compared to the deciduous species, at a value of 0.43 (p -value = 0.004, Dunn's test). Across the four phenophases, HIX was the only index that varied, marked by a significant reduction (0.45 compared to 0.72–0.76) during the emergence phase (p -value < 0.0001 Dunn's test; Table 3). In contrast, the FI, β : α , and BIX exhibited stability and remained largely unaffected by phenophase, with ranges of 1.38–1.44, 0.44–0.53, and 0.45–0.55, respectively (Table 3).

PARAFAC model

The validated PARAFAC model components (labeled as C#) (Fig. 2) were analyzed on a per species and per phenophase basis. Each identified component (Table 4) represents fluorescent compounds or groups of compounds whose fluorescence varies independently from the other components (Stedmon and Bro 2008). Statistically significant variations were observed in the distribution of component loadings across species and phenophases (Fig. 3). Yellow poplar exhibited notable differences from the other species in terms of C1 and C3 percent loadings (yellow poplar C1 = 26.69% and C3 = 43.31%, American beech/pitch pine/ sweet birch C1 = 30.88% and C3 = 34.10%; (p -value < 0.0001, Dunn's test; Fig. 3). Percent loading for C2 significantly differed (p -values ranged between < 0.0001 and 0.002, Dunn's test) among most species (American beech = 17.62%, sweet birch = 19.88%, yellow poplar = 17.41%,

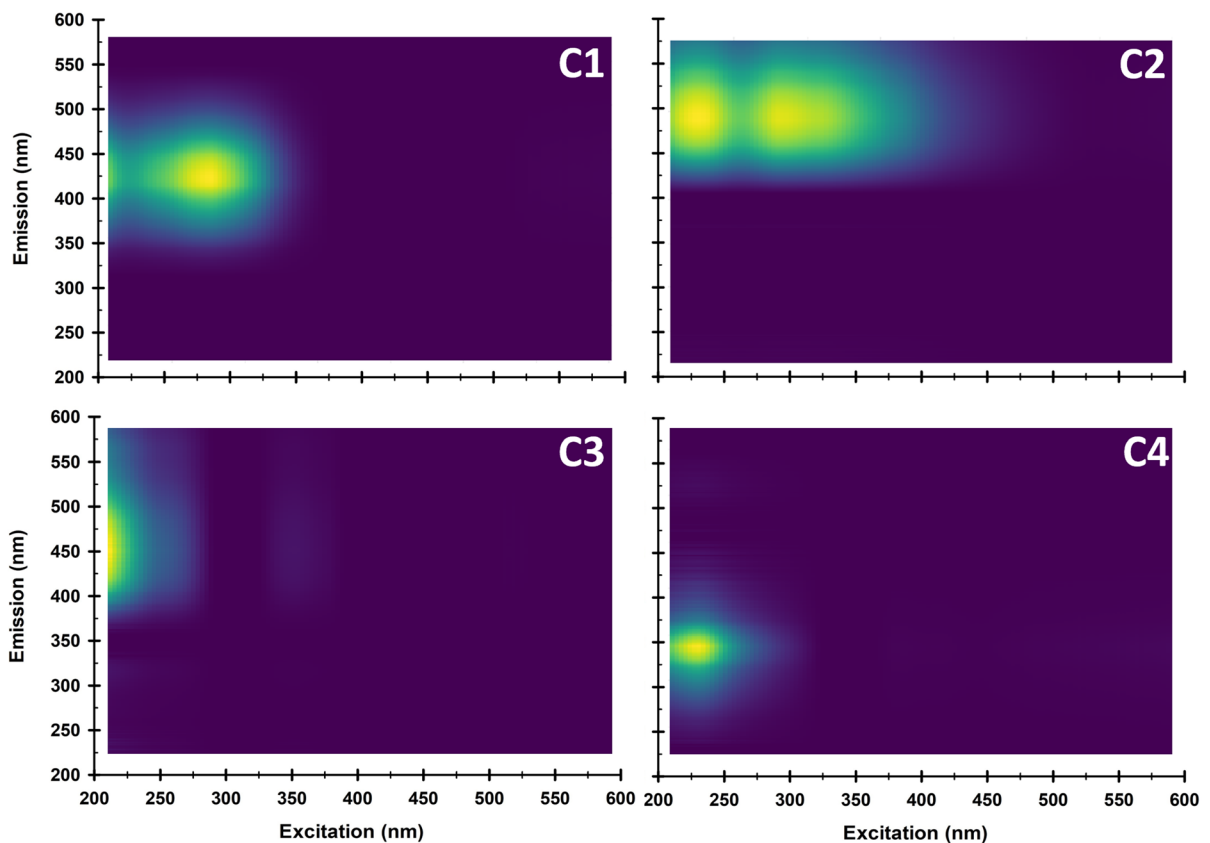
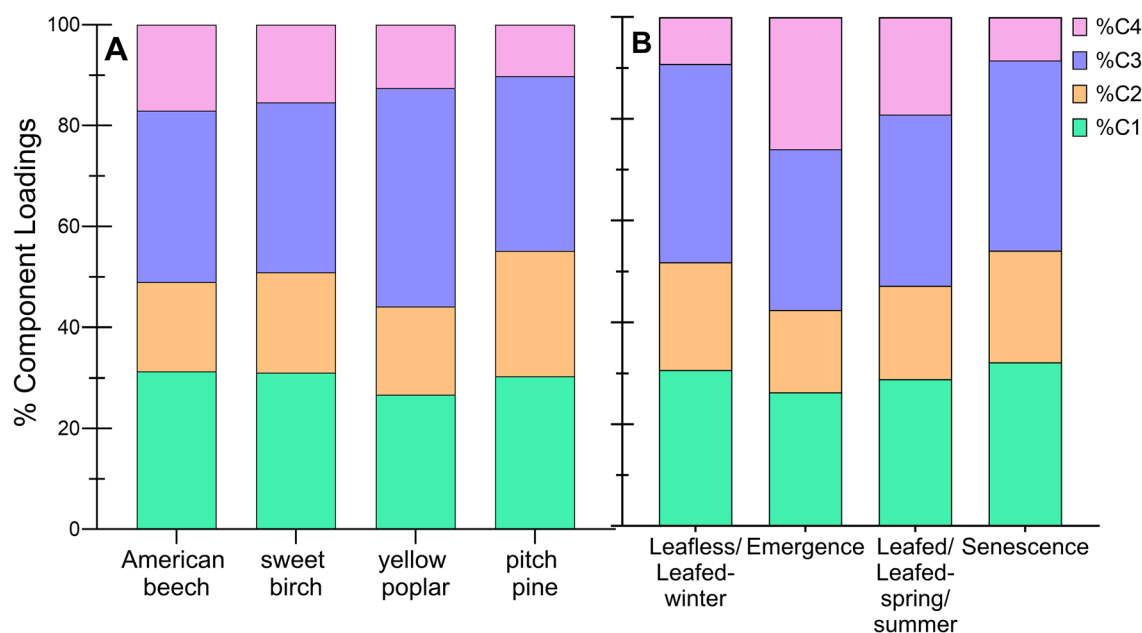


Fig. 2 4-component excitation-emission spectra for normalized stemflow parallel factor analysis model

Table 4 Components identified from PARAFAC model and their excitation and emission wavelength maxima

| Component | Excitation _{max} (nm)/emission _{max} (nm) | Component identifier |
|-----------|---|--------------------------------------|
| C1 | 330 / 415 | Microbial humic-like |
| C2 | 275, 345 / 490 | Terrestrial oxidized humic-like |
| C3 | 250 / 440 | Terrestrial reduced humic-like |
| C4 | 275/ 340 | Protein-like/small organic molecules |

**Fig. 3** **A** Species-specific (American beech, sweet birch, yellow poplar, and pitch pine) component loading percentage (C1, C2, C3 and C4) from all phenophases. **B** Phenophase-specific

leafless/leafed—winter, emergence, leafed/leafed—spring/summer, senescence) component loading percentage (C1, C2, C3 and C4) for all species

pitch pine=24.83%), except for American beech and yellow poplar (p -value=0.714, Dunn's test). C4 contribution was significantly distinct (p -value ranged between 0.014 to 0.025, Dunn's test) among pitch pine, American beech, and sweet birch (pitch pine=10.25%, American beech=17.06%, sweet birch=15.44%) (Fig. 3). Seasonally, C1, C2, and C4 displayed a consistent pattern, showing similarities between leafed/leafed-spring/summer and emergence (C1=27.56%, C2=17.24%, C4=22.48%), both of which were significantly different (p -value<0.0001 for all 3 components, Dunn's test) from the leafless/leafed-winter and senescence phenophases (C1=31.60%, C2=21.54%, C4=8.88%) (Fig. 3).

%C2 and %C3 are affected by both species and phenophase where the relative loadings of C2 and

C3 for American beech and sweet birch both follow the same general trend (emergence < leafed < senescence/leafless) while pitch pine follows a different trend with different loading values, suggesting the likelihood of electron transfer phenomena within the stemflow DOM that is both species and phenophase dependent (Fig. 4.; Table S2).

Discussion

Overall, we found statistically significant variations among tree species across a range of indices, including SUVA₂₅₄, E₂:E₃, S_R, BIX, HIX, and FI. For example, both HIX and SUVA₂₅₄ exhibit significant phenophase differences during emergence, while SUVA₂₅₄

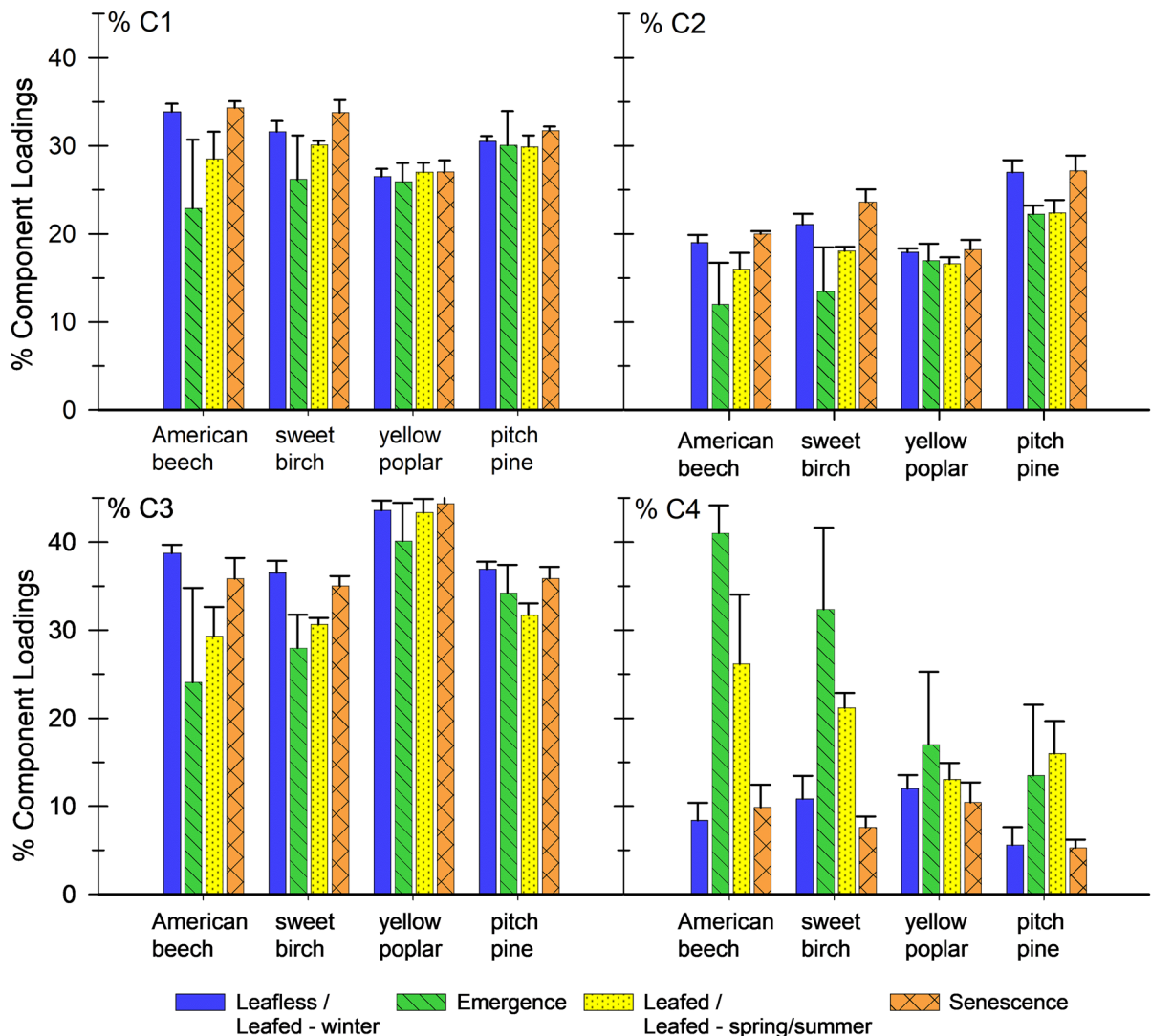


Fig. 4 Phenophase effect (leafless/leafed—winter, emergence, leafed/leafed—spring/summer, senescence) of each component loading mean percentage separated by each tree species

(American beech, sweet birch, yellow poplar, and pitch pine) with error bars denoting 95% confidence intervals

also exhibits a difference during senescence. These variations can be at least partially attributed to an influence of lignin degradation byproducts. The development of the PARAFAC model in this study that derives *solely* from stemflow DOM EEMs is the first to our knowledge. Of the four identified components, three (C1, C2, C4) display patterns with phenophase, which shed light on the relative distribution of specific aromatic moieties within stemflow DOM throughout different times of the year. The PARAFAC model also reveals interspecific differences,

notably, in the relative loadings of C2 and C3, which may indicate differences in the DOM redox states.

Stemflow DOM characterization by optical indices

Our stemflow optical indices are generally congruent with prior studies (see review by Chin et al. 2023), indicating a diversity of functional group types that could be attributed to microbial or terrestrial sources. Bacteria inhabiting corticular surfaces (Hudson et al. 2023), for example, could be a source of stemflow

DOM, while bacterial and hyphal feeders populating bark and associated epiphytic mosses and lichens (Ptatscheck et al. 2018) could also modify the carbon pool that contributes to stemflow DOM. For the optical indices based on absorbance, $SUVA_{254}$ values (standardized for comparison using the decadic absorption coefficient) of stemflow DOM samples fell within previously reported ranges of 1.9 to 6.2 L mg C⁻¹ m⁻¹ (Levia et al. 2012; Stubbins et al. 2017; Thieme et al. 2019). Generally, elevated values of $SUVA_{254}$ indicate greater proportions of aromatic moieties within the DOM (Chin et al. 1994). $E_2:E_3$ and S_R also fall within previously reported ranges (2.9 to 6.7 and 0.9 to 1.4 respectively; Levia et al. 2012). Differences in $E_2:E_3$ and S_R have correlated to differences with molecular mass in other studies (Helms et al. 2008), but it is not certain that this relationship necessarily applies in the same manner in the context of stemflow.

Likewise, the fluorescent indices are also consistent with previous literature. For example, FI (1.31 to 1.51), is within expected ranges reported for a variety of both terrestrial surface waters (Chin et al. 2023), and DOM end-member isolates (McKnight et al. 2001; Cawley et al. 2013). It is worth noting that the end-member values from isolates extracted from surface water sources (but not stemflow) fall within the range of our data. The FI corresponds to the spectral range associated with various quinoid moieties (Cory and McKnight 2005). Consequently, fluctuations in FI, given its nature as a ratio, signify shifts in the composition and/or relative proportion of these quinoid groups. Compositional differences may include: (1) variation in the specific molecules, such as lignin and varying extent of its degradation byproducts; (2) alterations in the redox states (which can impact fluorescence wavelengths); or (3) the presence of microbially derived material (Cory and McKnight 2005). For example, a lower FI can indicate terrestrially-derived matter (McKnight et al. 2001), such as that formed by decomposition of plant materials (Malcom 1990; McKnight et al. 2001). In the case of stemflow, such DOM may relate to humic substances released through the decomposition of bark (Guggenberger et al. 1994).

HIX reflects the relative fluorescence loading between the area of the EEM that includes humic peaks vs. the area where more amino-acid (protein) or small aromatics tend to fluoresce. In this study, HIX

ranges from 0.54 to 0.91, with an average of 0.77. These generally lower values indicate limited humification for the DOM (Ohno 2002), which is consistent with their origin in the canopy rather than the soil (D'Andrilli et al. 2022). It is, however, worth noting that humic acids are found in trees and absorb nutrients that promote robust growth (Fernandez-Escobar et al. 1996). For BIX, a range of values within 0.8 to 1.0 typically signifies the influence of microbial sources within DOM. Our findings are consistently below 0.6, which suggests a minimal contribution from microbial precursors (Hansen et al. 2016) and/or high concentrations of soluble lignin (Guggenberger and Zech 1994) which fluoresces at lower wavelengths, potentially overpowering microbial signals.

Stemflow DOM PARAFAC components

This is the first study to our knowledge to develop a PARAFAC model derived solely from stemflow EEMs. Identifying and characterizing stemflow DOM components in relation to other water systems generally implies that stemflow is a major source for hot spots, i.e., stemflow-influenced zones, such as near-trunk soils where stemflow may engender a disproportionately high rate of biogeochemical activity in the soil. Inamdar et al. (2012) found similar fluorescent components through PARAFAC in other environmental compartments at the Fair Hill Natural Resource Management Area, the same overall site as this study. For example, C5, one of their humic-like components, was quantified in litter, wetland soil water, shallow groundwater and deep groundwater. Stemflow, enriched with organic material from bark, leaves, and other canopy sources (e.g. aphid honeydew) delivers a concentrated pulse of carbon directly to the soil (Michalzik et al. 2016). This distinctive characteristic of stemflow underscores its significance as a concentrated input of carbon within localized areas around tree boles.

Components from the PARAFAC model matched 172 previously reported components (>0.95 similarity score) in the OpenFluor database (Murphy et al. 2014). Based on these similarities, C1 is identified as consistent with others derived from microbially derived “humic-like” or “fulvic-like” compounds (Garcia et al. 2015; Li et al. 2016; Zhuang et al. 2022). This is a group of chemical compounds that fluoresce in a region in which decomposed plant

material typically fluoresces, which would explain an increase in C1 across all species during senescence. C2 is identified as consistent with an oxidized humic-like peak and C3 as consistent with a reduced humic-like peak, which matches fluorescent components from other terrestrially sourced DOM (Stedmon et al. 2003; Yamashita et al. 2011; Lambert et al. 2016; Imbeau et al. 2021). C4 is identified as consistent with a protein-like, low molecular weight peak (Osburn et al. 2016; Wheeler et al. 2017; Cabrera et al. 2020; Ryan et al. 2022). Several compounds containing different fluorophores are known to fluoresce in this region with similar signature to proteins and amino acids (Aiken 2014). Tannins and lignin phenols are among these compounds (Aiken 2014), which are commonly found in the bark of the trees (Guggenberger et al. 1994).

Species variation in DOM characterization

In general, stemflow serves as a transport vehicle for nutrient-rich and bioavailable inputs into the forest floor, and these “hot spots” of concentrated material may play a number of ecologically important roles, such as affecting the microbial diversity in near-stem soils (Rosier et al. 2016). Different plant species will contribute to this influx of nutrients and materials from stemflow to various extents, depending on both canopy structural characteristics and precipitation regime (Levia and Frost 2003). Thus, the species-specific stemflow composition is critical in understanding where and to what degree such hot spots may occur in a forested ecosystem. For instance, stemflow composition and fluxes of major cations and organically bound C, N, and S from European beech are influenced by low infestation levels of aphids, which, in turn, affect the trophic interactions in the phyllosphere (Michalzik et al. 2016).

An example of species variation with stemflow DOM is that yellow poplar and pitch pine exhibit higher $SUVA_{254}$ values compared to sweet birch and American beech trees. These elevated values suggest greater proportions of aromatic compounds (Chin et al. 1994) within stemflow (Table 2). The primary source of these aromatic substances in stemflow DOM is believed to be lignin and its degradation products, major polyphenolic components of vascular plants that are washed from tree

surfaces (Guggenberger and Zech 1994), particularly bark (Guggenberger et al. 1994). Yellow poplar also exhibits the highest $E_2:E_3$ ratio, indicative of lower molecular mass solutes, possibly containing lignin byproducts that are degraded to a further extent. This is consistent with having higher-normalized absorbance around 254 nm, which would increase $SUVA_{254}$ as well. In contrast, American beech shows the opposite trend with respect to both $SUVA_{254}$ and $E_2:E_3$ (Levia et al. 2012), suggesting the lignin in its stemflow is less degraded.

Garcia et al. (2015) reported a decline in C1 in surface water of a forested catchment during emergence, consistent with our observations in American beech. The site primarily featured *Nothofagus pumilio*, a member of the Fagaceae family, suggesting that deciduous tree species in the vicinity of catchments can influence DOM composition, specifically C1 and FI. Our findings exhibit significant variation among species, specifically with American beech having the highest FI. It is unclear whether stemflow C1's relationship holds for other species within the Fagaceae family.

Pitch pine has the lowest S_R and is the only statistically different value from the other species (Table 2). A possible explanation for this is the presence of terpenes in coniferous trees. Certain terpenes such as myrcene, terpinene, and pinene, absorb at longer wavelengths (Bones et al. 2009), which would influence the denominator of the S_R (Table 1). Pinene is the most prominent terpene in pitch pine (Son et al. 2015).

In terms of fluorescent components, pitch pine stemflow also stands out from the other tree species. C4 is significantly different between pitch pine and sweet birch, although the precise reason for this is unclear. However, all species show unique differences between C2 and C3 relative loadings across phenophases (Fig. 4). As these components are consistent with oxidized/reduced humic-like materials, fluctuations in the extent of oxidation on a per-species and per-phenophase basis demonstrates a potential cyclic yearly relationship for each tree species. Such findings may demonstrate the impact of redox moieties on variations in DOM among tree species, perhaps by comparing C2 and C3 loadings to understand quinone composition on near-trunk soils.

Phenophase variation in DOM characterization

Stemflow is a significant driver of carbon cycling dynamics (Ryan et al. 2022). Seasonal variation underscores how hot moments, triggered by changes in seasons, intensify the flow of water down tree trunks, enhancing the leaching of organic matter and enriching stemflow with carbon-rich compounds. Ultimately, these “hot moments”, temporal events caused by factors such as temperature, amplify carbon fluxes through stemflow, affecting soil carbon dynamics, microbial activity, and decomposition rates. We observe that phenophases alter the carbon composition in stemflow, consistent with previous work by Levia et al. (2012) with stemflow absorbance, Ryan et al. (2022) in a throughfall/precipitation/ stemflow model, and Wheeler et al. (2017) in a litter leachate model.

During senescence, $SUVA_{254}$ values are highest (Table 3), indicating increased entrainment of aromatic carbon, such as lignin and its byproducts, as leaves drop and scar tissue forms to protect branches. Compared to Ryan et al. (2022), who observed no trend, and Wheeler et al. (2017), with senescence being the lowest in litter leachate, this observation is unique to stemflow. In contrast, $SUVA_{254}$ is lowest during emergence (Table 3), suggesting that either (1) lignin utilization and other necessary chemical species for leaf formation; or (2) lignin is potentially less degraded (i.e., fewer molecules absorbing at 254 nm). Among the deciduous species investigated, a drop in HIX was observed during emergence. One explanation for this decrease may be the quenching of fluorescence by Fe (II), causing a shift toward shorter wavelengths (Jia et al. 2021). Bennet and Oserkowsky (1933) showed a rapid rise in iron concentrations in sap flux in early spring before stabilizing to a lower concentration for the rest of the year, similar to the trend for HIX witnessed in this study. It could also reflect an increase in components that fluoresce in the protein-like region, perhaps derived from amino acids or other small molecules. However, in the case of pitch pine, variations in HIX were evident during both senescence and emergence (Fig. S5). Interestingly, we observed no significant changes in $E_2:E_3$ and S_R between phenophases, suggesting consistent degradation of lignin within a species. The FI and BIX did not show trends either, suggesting that the components of DOM that give rise to those regions

where those indices derive are more consistent throughout the year.

Prior research indicates that during the leafless season, an absence of foliage and lower air temperatures enhances stemflow-bark contact time (Levia and Frost 2003), thereby increasing $SUVA_{254}$ (Levia et al. 2012), consistent with our study which also shows $SUVA_{254}$ increasing with the onset of lower air temperatures during senescence (Table 3), although winter $SUVA_{254}$ values were lower, possibly due to the inclusion of the evergreen pitch pine. C1, C2, and C4 also exhibited seasonal groupings, with leafed/leafed-spring/summer and emergence phases differing significantly from leafless/leafed-winter and senescence phases. This observation suggests that the components in stemflow DOM undergo seasonal patterns despite not being revealed by the other fluorescent indices above, which may be due to those indices being largely defined as ratios, so a lack of change in FI, BIX, etc. could be from a counterbalance of component shifts. C1 and C2 both increase during the leafless/leafed-winter phenophase (leafed to leafless, C1 ~27% to 31%, C2 ~17% to 21%) but C4 decreases during that time (C4 ~22% to 8%). Part of the reason for this may be the increased influence of substantial quantities of canopy-based biodegradable, hydrophilic neutral carbohydrates during the leafed season creating an increase in microbial activity feeding on the carbon pool. This increase in activity will alter the type of carbon observed and change the proportions of components (Guggenberger and Zech 1994; Michalzik et al. 2001). The higher percentage of C4 in stemflow during emergence and the leafed season may be partly due to the larger aboveground surface areas (both foliar and woody) compared to dormancy, leading to the degradation and leaching of diverse and complex aromatics, including lignin and tannins (Guggenberger et al. 1994), which fluoresce in this region.

Further research is required to validate a relationship between $E_2:E_3$ and solute molecular mass in stemflow. $E_2:E_3$ is largely species but not phenophase dependent in this study, raising an interesting question as to what this index actually indicates in stemflow. Perhaps it is simply a marker of conjugation, as more conjugated molecules (longer polyphenolic polymer chains) will absorb at higher wavelengths, which could be consistent with extent of lignin degradation. Also, the precise factors contributing to HIX

variations in emergence remain unclear, but further experiments on humic substances and iron concentrations in different species throughout the four phenophases is recommended to understand the *in-situ* processes utilizing humic substances for regrowth during emergence in these species.

Conclusion

The study illuminates the role of stemflow in the transfer of water and solutes to the floor of forest ecosystems that likely help contour near-trunk water and biogeochemical cycling. A comprehensive analysis of the absorbance and fluorescent signatures of stemflow DOM across different phenophases of four major tree species in temperate eastern forests has shown that aromatic, metal-binding, and large molecular mass solutes play a significant role in stemflow DOM. Further, this study developed a stemflow-specific PARAFAC model that identified key components in stemflow DOM and their relationship with different species, which offers a deeper understanding of stemflow's chemical composition and its potential in creating localized hot spots and hot moments in near-trunk soils. The findings confirm the presence of aromatic DOM compounds in stemflow, partly derived from lignin and its degradation products. Significant variations in DOM properties among tree species and phenophases were observed, highlighting the importance of species-specific analyses and the impact of phenological shifts on stemflow DOM quality.

The stemflow-specific PARAFAC model has yielded insights, such as identifying components, cyclic redox relationships, and seasonal patterns, on the composition and dynamics of stemflow DOM across different tree species and phenophases. The model has identified four components, with C1 representing microbially derived "humic-like" or "fulvic-like" compounds, exhibiting increased presence across all species during senescence. C2 was identified as an oxidized humic-like peak, while C3 represented a reduced humic-like peak, aligning with fluorescent components found in other terrestrially-sourced DOM. Additionally, C4 was characterized as a protein-like, low molecular weight peak. Besides interspecific differences, C1, C2, and C4 display patterns with phenophase, which shed light on the relative distribution of specific aromatic moieties within

stemflow DOM throughout different times of the year, and in general reveal more variation than ratios from fluorescence indices alone can describe, providing a more specific understanding of shifts in molecular composition with respect to stemflow processes. The study raises questions about the relationships between certain fluorescent components of stemflow DOM, such as the interplay between oxidized and reduced quinones and their potential cyclic interactions within certain species. This research provides valuable insights into the finer temporal variations that help reveal carbon cycling dynamics with respect to phenophase.

Acknowledgements This research was financially supported by the National Science Foundation (NSF GCR CMMI 1934887). We extend our gratitude to the Fair Hill NRMA staff for facilitating access to the study site. Special appreciation is directed towards Sara Haney and Dillon Siple for their indispensable contributions to conducting analyses and sample collection at the research site. We acknowledge and thank the UD GCR team for their valuable collaborations and feedback, which contributed to the advancement of this study. J. Guerard received support from the Naval Academy Research Council (NARC) program at the US Naval Academy, funded by the Office of Naval Research (ONR). We would like to convey our appreciation to the Editors of the journal and the anonymous reviewers for their constructive and insightful feedback on the manuscript. Initial efforts for this paper stem from RO's MS thesis.

Author contributions RO and DL conceived and designed the study. Material preparation and data collection was performed by RO. Analysis was performed by all authors. The first draft of the manuscript was written by RO and all authors commented on previous versions of the manuscript.

Funding Funding was provided by National Science Foundation Grant no. 1934887.

Data availability The stemflow-specific PARAFAC model developed for this study is available on openfluor.org.

Declarations

Competing interests The authors have no relevant financial or non-financial interests to disclose.

Open Access This article is licensed under a Creative Commons Attribution 4.0 International License, which permits use, sharing, adaptation, distribution and reproduction in any medium or format, as long as you give appropriate credit to the original author(s) and the source, provide a link to the Creative Commons licence, and indicate if changes were made. The images or other third party material in this article are included in the article's Creative Commons licence, unless indicated otherwise in a credit line to the material. If material is not

included in the article's Creative Commons licence and your intended use is not permitted by statutory regulation or exceeds the permitted use, you will need to obtain permission directly from the copyright holder. To view a copy of this licence, visit <http://creativecommons.org/licenses/by/4.0/>.

References

- Aiken GR (2014) A chemist's perspective. In: Coble P, Lead J, Baker A, Reynolds D, Spencer RGM (eds) *Aquatic organic matter fluorescence*. Cambridge University Press, Cambridge, pp 75–122
- Bennett JP, Oserkowsky J (1933) Copper and iron in the tracheal sap of deciduous trees. *Am J Bot* 20(10):632–637. <https://doi.org/10.2307/2436126>
- Bones DL, Henricksen DK, Mang SA, Gonsior M, Bateman AP, Nguyen TB, Cooper WJ, Nizkorodov SA (2010) Appearance of strong absorbers and fluorophores in limonene-O₃ secondary organic aerosol due to NH₄⁺-mediated chemical aging over long time scales. *J Geophys Res* 115:D05203. <https://doi.org/10.1029/2009jg1012864>
- Cabrera JM, García PE, Pedrozo FL, Queimaliños CP (2020) Dynamics of the dissolved organic matter in a stream-lake system within an extremely acid to neutral pH range: Agrio-Caviahue watershed. *Spectrochim Acta A* 235:118278. <https://doi.org/10.1016/j.saa.2020.118278>
- Carlyle-Moses DE, Iida S, Germer S, Llorens P, Michalzik B, Nanko K, Tischer A, Levia DF (2018) Expressing stemflow commensurate with its ecophysiological importance. *Adv Water Resour* 121:472–479. <https://doi.org/10.1016/j.advwatres.2018.08.015>
- Cawley KM, McKnight DM, Miller P, Cory R, Fimmen RL, Guerard J, Diesler M, Jaros C, Chin YP, Foreman C (2013) Characterization of fulvic acid fractions of dissolved organic matter during ice-out in a hyper-eutrophic, coastal pond in Antarctica. *Environ Res Lett* 1;8(4):045015. <https://doi.org/10.1088/1748-9326/8/4/045015>
- Cayuela C, Levia DF, Latron J, Llorens P (2019) Particulate matter Fluxes in a Mediterranean mountain forest: Inter-specific differences between throughfall and stemflow in oak and pine stands. *J Geophys Res* 124:5106–5116. <https://doi.org/10.1029/2019JD030276>
- Chen S, Cao R, Yoshitake S, Ohtsuka T (2019) Stemflow hydrology and DOM flux in relation to tree size and rainfall event characteristics. *Agric For Meteorol* 279:107753. <https://doi.org/10.1016/j.agrformet.2019.107753>
- Chin YP, Aiken GR, O'Loughlin E (1994) Molecular weight, Polydispersity, and spectroscopic properties of Aquatic Humic Substances. *Environ Sci Technol* 28:1853–1858. <https://doi.org/10.1021/es00060a015>
- Chin YP, McKnight DM, D'Andrilli J, Brooks N, Cawley K, Guerard J, Perdue EM, Stedom CA, Tratnyek PG, Westerhoff P, Wozniak AS, Bloom PR, Foreman C, Gabor R, Hamdi J, Hanson B, Hozalski RM, Kellerman A, McKay G, Silverman V, Spencer RGM, Ward C, Xin D, Rosario-Ortiz F, Remucal CK, Reckhow D (2023) Identification of next-generation International Humic Substances Society reference materials for advancing the understanding of the role of natural organic matter in the Anthropocene. *Aquat Sci* 85:32. <https://doi.org/10.1007/s00027-022-00923-x>
- Cooper KJ, Whitaker FF, Anesio AM, Naish M, Reynolds DM, Evans EL (2016) Dissolved organic carbon transformations and microbial community response to variations in recharge waters in a shallow carbonate aquifer. *Biogeochem* 129:215–234. <https://doi.org/10.1007/s10533-016-0226-4>
- Cory RM, McKnight DM (2005) Fluorescence spectroscopy reveals ubiquitous presence of oxidized and reduced quinones in dissolved organic matter. *Environ Sci Technol* 39:8142–8149. <https://doi.org/10.1021/es0506962>
- Cory RM, McNeill K, Cotner JP, Amado A, Purcell JM, Marshall AG (2010) Singlet oxygen in the coupled photochemical and biochemical oxidation of dissolved organic matter. *Environ Sci Technol* 44:3683–3689. <https://doi.org/10.1021/es902989y>
- D'Andrilli J, Silverman V, Buckley S, Rosario-Ortiz FL (2022) Inferring ecosystem function from dissolved organic matter optical properties: a critical review. *Environ Sci Technol* 56(16):11146–61. <https://doi.org/10.1021/acs.est.2c04240>
- Fernandez-Escobar R, Benlloch M, Barranco D, Duenas A, Gutierrez Ganan JA (1996) Response of olive trees to foliar application of humic substances extracted from leonardite. *Sci Hortic* 66:191–200. [https://doi.org/10.1016/S0304-4238\(96\)00914-4](https://doi.org/10.1016/S0304-4238(96)00914-4)
- Garcia RD, Reissig M, Queimaliños CP, Dieguez MC (2015) Climate-driven terrestrial inputs in ultraoligotrophic mountain streams of Andean Patagonia revealed through chromophoric and fluorescent dissolved organic matter. *Sci Total Environ* 521–522:280–292. <https://doi.org/10.1016/j.scitotenv.2015.03.102>
- Guggenberger G, Zech W (1994) Composition and dynamics of dissolved carbohydrates and lignin-degradation products in two coniferous forests, N.E. Bavaria, Germany soil. *Biol Biochem* 26:19–27. [https://doi.org/10.1016/0038-0717\(94\)90191-0](https://doi.org/10.1016/0038-0717(94)90191-0)
- Guggenberger G, Zech W, Schulten H-R (1994) Formation and mobilization pathways of dissolved organic matter: Evidence from chemical structural studies of organic matter fractions in acid forest floor solutions. *Org Geochem* 21:51–66. [https://doi.org/10.1016/0146-6380\(94\)90087-6](https://doi.org/10.1016/0146-6380(94)90087-6)
- Hansen AM, Kraus TE, Pellerin BA, Fleck JA, Downing BD, Bergamaschi BA (2016) Optical properties of dissolved organic matter (DOM): effects of biological and photolytic degradation. *Limnol Oceanogr* 61:1015–1032. <https://doi.org/10.1002/lno.10270>
- Helms JR, Stubbins A, Ritchie JD, Minor EC, Kieber DJ, Mopper K (2008) Absorption spectral slopes and slope ratios as indicators of molecular weight, source, and photobleaching of chromophoric dissolved organic matter. *Limnol Oceanogr* 53:955–969. <https://doi.org/10.4319/lno.2008.53.3.0955>
- Hudson JE, Levia DF, Yoshimura KM, Gittel NR, Hudson SA, Biddle JF (2023) Mapping bark bacteria: initial insights of stemflow-induced changes in bark surface phyla. *Microbiol Spectr* 11(6):e03562-23. <https://doi.org/10.1128/spectrum.03562-23>
- Huguet AL, Vacher L, Relexans S, Saubusse S, Froidefond JM, Parlanti E (2009) Properties of fluorescent dissolved

- organic matter in the Gironde Estuary. *Org Geochem* 40:706–719. <https://doi.org/10.1016/j.orggeochem.2009.03.002>
- Imbeau E, Vincent WF, Wauthy M, Cusson M, Rautio M (2021) Hidden stores of organic matter in northern lake ice: Selective retention of terrestrial particles, phytoplankton and labile carbon. *J Geophys Res Biogeosci* 126:e2020JG006233. <https://doi.org/10.1029/2020jg006233>
- Inamdar S, Finger N, Singh S, Mitchell M, Levia D, Bais H, Scott D, McHale P (2012) Dissolved organic matter (DOM) concentration and quality in a forested mid-Atlantic watershed, USA. *Biogeochemistry* 108:55–76. <https://doi.org/10.1007/s10533-011-9572-4>
- Jia K, Manning CC, Jollymore A, Beckie R (2021) Technical Note: Effects of Iron(II) on fluorescence properties of dissolved organic matter at circumneutral pH. *Hydrol Earth Syst Sci* 25:4983–4993. <https://doi.org/10.5194/hess-25-4983-2021>
- Kalbitz K, Geyer S, Geyer W (2000) A comparative characterization of dissolved organic matter by means of original aqueous samples and isolated humic substances. *Chemosphere* 40:1305–1312. [https://doi.org/10.1016/S0045-6535\(99\)00238-6](https://doi.org/10.1016/S0045-6535(99)00238-6)
- Lambert T, Bouillon S, Darchambeau F, Massicotte P, Borges AV (2016) Shift in the chemical composition of dissolved organic matter in the Congo River network. *J Geophys Res Biogeosci* 13:5405–5420. <https://doi.org/10.5194/bg-13-5405-2016>
- Levia DF, Frost EE (2003) A review and evaluation of stemflow literature in the hydrologic and biogeochemical cycles of forested and agricultural ecosystems. *J Hydrol* 274:1–29. [https://doi.org/10.1016/S0022-1694\(02\)00399-2](https://doi.org/10.1016/S0022-1694(02)00399-2)
- Levia DF, Germer S (2015) A review of stemflow generation dynamics and stemflow-environment interactions in forests and shrublands. *Rev Geophys* 53:673–714. <https://doi.org/10.1002/2015rg000479>
- Levia DF, Van Stan JT, Mage SM, Kelley-Hauske PW (2010) Temporal variability of stemflow volume in a beech-yellow poplar forest in relation to tree species and size. *J Hydrol* 380:112–120. <https://doi.org/10.1016/j.jhydrol.2009.10.028>
- Levia DF, Van Stan II JT, Inamdar SP, Jarvis MT, Mitchell MJ, Mage SM, Scheick CE, Mchale PJ (2012) Stemflow and dissolved organic carbon cycling: temporal variability in concentration, flux, and UV-Vis spectral metrics in a temperate broadleaved deciduous forest in the eastern United States. *Can J For Res* 42:207–216. <https://doi.org/10.1139/x11-173>
- Levia DF, Bischoff S, Gruselle M, Nätke K, Legates DR, Lutgen A, Boyer EW, Michalzik B (2023) Geometric configurations of particulate matter in terrestrial solutions of a temperate beech forest. *J Aerosol Sci* 172:106196. <https://doi.org/10.1016/j.jaerosci.2023.106196>
- Levia DF, Keim RF, Carlyle-Moses DE, Frost EE (2011), Throughfall and stemflow in wooded ecosystems. In: Levia DF, Carlyle-Moses D, Tanaka T (eds) *Forest hydrology and biogeochem*. Springer, London, pp 425–443. https://doi.org/10.1007/978-94-007-1363-5_21
- Li P, Lee SH, Lee SH, Lee JB, Lee YK, Shin H-S, Hur J (2016) Seasonal and storm-driven changes in chemical composition of dissolved organic matter: a case study of a reservoir and its forested tributaries. *Environ Sci Pollut Res* 23:24834–24845. <https://doi.org/10.1007/s11356-016-7720-z>
- Llorens P, Latron J, Carlyle-Moses DE, Nätke K, Chang JL, Nanko K, Iida S, Levia DF (2022) Stemflow infiltration areas into forest soils around American beech (*Fagus grandifolia* Ehrh.) trees. *Ecohydrology* 15(2):2369. <https://doi.org/10.1002/eco.2369>
- Malcom RL (1990) The uniqueness of humic substances in each of soil, stream and marine environments. *Anal Chim Acta* 232:19–30. [https://doi.org/10.1016/S0003-2670\(00\)81222-2](https://doi.org/10.1016/S0003-2670(00)81222-2)
- McDowell WH, Pérez-Rivera KX, Shaw ME (2020). Assessing the ecological significance of throughfall in forest ecosystems. In Levia DF, Carlyle-Moses DE, Iida S, Michalzik B, Nanko K, Tischer A (eds) *Forest-Water Interactions*, Springer Nature Switzerland, Cham, pp 299–318. https://doi.org/10.1007/978-3-030-26086-6_13
- McKnight DM, Boyer EW, Westerhoff PK, Doran PT, Kulbe T, Andersen DT (2001) Spectrofluorometric characterization of dissolved organic matter for indication of precursor organic material and aromaticity. *Limnol Oceanogr* 46:38–48. <https://doi.org/10.4319/lo.2001.46.1.0038>
- Michalzik B, Kalbitz K, Park JH, Solinger S, Matzner E (2001) Fluxes and concentrations of dissolved organic carbon and nitrogen – a synthesis for temperate forests. *Biogeochem* 52(2):173–205. <https://doi.org/10.1023/A:1006441620810>
- Michalzik B, Levia DF, Bischoff S, Nätke K, Richter S (2016) Effects of aphid infestation on the biogeochemistry of the water routed through European Beech (*Fagus sylvatica* L.) Saplings. *Biogeochem* 129(12):197–214
- Murphy KR, Stedmon CA, Wenig P, Bro R (2014) OpenFluor – an online spectral library of auto-fluorescence by organic compounds in the environment. *Anal Methods* 6:658–661. <https://doi.org/10.1039/c3ay41935e>
- Ohno T (2002) Fluorescence inner-filtering correction for determining the humification index of dissolved organic matter. *Environ Sci Technol* 36:742–746. <https://doi.org/10.1021/es0155276>
- Osburn CL, Boyd TJ, Montgomery MT, Bianchi TS, Coffin RB, Paerl HW (2016) Optical proxies for terrestrial dissolved organic matter in estuaries and coastal waters. *Front Mar Sci*. <https://doi.org/10.3389/fmars.2015.00127>
- Parker GG (1983) Throughfall and stemflow in the forest nutrient cycle. *Adv Ecol Res*. [https://doi.org/10.1016/S0065-2504\(08\)60108-7](https://doi.org/10.1016/S0065-2504(08)60108-7)
- Parlanti EK, Worz L, Geoffroy L, Lamotte M (2000) Dissolved organic matter fluorescence spectroscopy as a tool to estimate biological activity in a coastal zone submitted to anthropogenic inputs. *Org Geochem* 31:1765–1781. [https://doi.org/10.1016/S0146-6380\(00\)00124-8](https://doi.org/10.1016/S0146-6380(00)00124-8)
- Peuravuori J, Pihlaja K (1997) Molecular size distribution and spectroscopic properties of aquatic humic substances. *Anal Chim Acta* 337:133–149. [https://doi.org/10.1016/S0003-2670\(96\)00412-6](https://doi.org/10.1016/S0003-2670(96)00412-6)
- Ptatscheck C, Milne PC, Traunspurger W (2018) Is stemflow a vector for the transport of small metazoans from tree

- surfaces down to soil? *BMC Ecol* 18(1):43. <https://doi.org/10.1186/s12898-018-0198-4>
- Pucher M, Wunsch U, Weigelhofer G, Murphy K, Hein T (2019) staRdom: Versatile software for analyzing spectroscopic data of dissolved organic matter in R. *Water* 11:2366. <https://doi.org/10.3390/w11112366>
- Rosier CL, Levia DF, Van Stan JT, Aufdenkampe A, Kan J (2016) Seasonal dynamics of the soil microbial community structure within the proximal area of tree boles: possible influence of stemflow. *Eur J Soil Biol* 73:108–118. <https://doi.org/10.1016/j.ejsobi.2016.02.003>
- Ryan KA, Adler T, Chalmers AT, Perdrial J, Sebestyen S, Shanley JB, Stubbins A (2022) Optical properties of dissolved organic matter in throughfall and stemflow vary across tree species and season in a temperate headwater forest. *Biogeochem* 165:53–72. <https://doi.org/10.1007/s10533-022-00985-x>
- Shigihara A, Matsumoto K, Sakurai N, Igawa M (2008) Leaching of cell wall components caused by acid deposition on fir needles and trees. *Sci Total Environ* 398:185–195. <https://doi.org/10.1016/j.scitotenv.2008.03.007>
- Siegert CM, Levia DF, Hudson SA, Downtin AL, Zhang F, Mitchell MJ (2016) Small-scale topographic variability influences tree species distribution and canopy throughfall partitioning in a temperate deciduous forest. *For Ecol Manag* 359:109–117. <https://doi.org/10.1016/j.foreco.2015.09.028>
- Siegert CM, Levia DF, Leathers DJ, Van Stan JT, Mitchell MJ (2017) Do storm synoptic patterns affect biogeochemical fluxes from temperate deciduous forest canopies? *Biogeochemistry* 132:273–292. <https://doi.org/10.1007/s10533-017-0300-6>
- Son Y-S, Kim K-J, Jung I-H, Lee S-J, Kim J-C (2015) Seasonal variations and emission fluxes of monoterpene emitted from coniferous trees in East Asia: Focused on *Pinus rigida* and *pinus koraiensis*. *J Atmos Chem* 72:27–41. <https://doi.org/10.1007/s10874-015-9303-7>
- Stedmon CA, Bro R (2008) Characterizing dissolved organic matter fluorescence with parallel factor analysis: a tutorial. *Limnol Oceanogr Meth* 6:572–579. <https://doi.org/10.4319/lom.2008.6.572>
- Stedmon CA, Markager S, Bro R (2003) Tracing dissolved organic matter in aquatic environments using a new approach to fluorescence spectroscopy. *Mar Chem* 82:239–254. [https://doi.org/10.1016/s0304-4203\(03\)00072-0](https://doi.org/10.1016/s0304-4203(03)00072-0)
- Stubbins A, Silva LM, Dittmar T, Van Stan JT (2017) Molecular and optical properties of tree-derived dissolved organic matter in throughfall and stemflow from live oaks and eastern red cedar. *Front Earth Sci*. <https://doi.org/10.3389/feart.2017.00022>
- Thieme L, Graeber D, Hofmann D, Bischoff S, Scharz MT, Steffen B, Meyer U-N, Kaupenjohann M, Wilcke W, Michalzik B, Siemens J (2019) Dissolved organic matter characteristics of deciduous and coniferous forests with variable management: Different at the source, aligned in the soil. *J Geophys Res Biogeosci* 16:1411–1432. <https://doi.org/10.5194/bg-16-1411-2019>
- U.S. Climate Normals (2023) In: NOAA NCEI U.S. Climate Normals Quick Access. <https://www.ncei.noaa.gov/access/us-climate-normals/#dataset=normals-annualseasonal&timeframe=30&location=DE&station=USC00076410>. Accessed 9 Jun 2023
- Van Stan JT, Wagner S, Guillemette F, Whitetree A, Lewis J, Silva L, Stubbins A (2017) Temporal dynamics in the concentration, flux, and optical properties of tree-derived dissolved organic matter in an epiphyte-laden oak-cedar forest. *J Geophys Res Biogeosci* 122:2982–2997. <https://doi.org/10.1002/2017jg004111>
- Wagner S, Brantley S, Stuber S, Van Stan J, Whitetree A, Stubbins A (2019) Dissolved black carbon in throughfall and stemflow in a fire-managed longleaf pine woodland. *Biogeochem*. <https://doi.org/10.1007/s10533-019-00620-2>
- Weishaar JL, Aiken GR, Bergamaschi BA, Fram MS, Fujii R, Mopper K (2003) Evaluation of specific ultraviolet absorbance as an indicator of the chemical composition and reactivity of dissolved organic carbon. *Environ Sci Technol* 37:4702–4708. <https://doi.org/10.1021/es030360x>
- Wheeler KI, Levia DF, Hudson JE (2017) Tracking senescence-induced patterns in leaf litter leachate using parallel factor analysis (PARAFAC) modeling and self-organizing maps. *J Geophys Res Biogeosci* 122:2233–2250. <https://doi.org/10.1002/2016jg003677>
- Wilson HF, Xenopoulos MA (2009) Effects of agricultural land use on the composition of fluvial dissolved organic matter. *Nat Geosci* 2:37–41. <https://doi.org/10.1038/ngeo391>
- Yamashita Y, Kloeppel BD, Knoepp J, Zausen GL, Jaffe R (2011) Effects of watershed history on dissolved organic matter characteristics in headwater streams. *Ecosystems* 14:1110–1122. <https://doi.org/10.1007/s10021-011-9469-z>
- Zhuang W-E, Chen W, Yang L (2022) Effects of photodegradation on the optical indices of chromophoric dissolved organic matter from typical sources. *Int J Environ Res Public Health* 19:14268. <https://doi.org/10.3390/ijerph192114268>

Publisher's Note Springer Nature remains neutral with regard to jurisdictional claims in published maps and institutional affiliations.